*IOSR Journal of Biotechnology and Biochemistry (IOSR-JBB)*
*ISSN: 2455-264X, Volume 11, Issue 5 Series 1 (Sept. – Oct. 2025), PP 21-36*
*www.iosrjournals.org*

# Structure -Based Inhibitor Design Targeting IDH1-R132Q In Glioblastoma Using Drug Discover With Biopython

Namit Narang, Uma Kumari, Avirup Dey, Adarsh Murali
*Project Trainee At Bioinformatics Project And Research Institute, Noida - 201301, India*
*Senior Bioinformatics Scientist, Bioinformatics Project And Research Institute, Noida - 201301, India*
*Project Trainee At Bioinformatics Project And Research Institute, Noida - 201301, India*
*Project Trainee At Bioinformatics Project And Research Institute, Noida - 201301, India*

***Abstract:***
*In order to find novel inhibitors that target the Isocitrate Dehydrogenase 1 R132Q mutant (IDH1-R132Q), a major oncogenic driver in secondary glioblastoma (GBM), this paper describes a Structure-Based Drug Design (SBDD) approach. We described the allosteric regulatory site using the high-resolution X-ray crystal structure (PDB: 8VHB), which was confirmed by strict quality metrics (ERRAT: 97.9%; PROCHECK: 91.4% preferred). The best binding pocket, C1, was found by computational analysis to have a large cavity volume (9201 $A^03$) and the highest predicted affinity (Vina score: -9.9 kcal/mol). Both natural compounds and well-established clinical candidates were assessed using comparative molecular docking against this crucial dimer interface site. According to the results, the natural product Withaferin A had the highest theoretical binding affinity (-10.2 kcal/mol), which was much higher than that of the approved inhibitor Olutasidenib (-9.2 kcal/mol) and the clinical benchmark Safusidenib (DS-1001b, -9.9 kcal/mol). Withaferin A's engagement of crucial allosteric residues (GLN90, TYR139, and ARG140) necessary for enzyme regulation was verified by interaction analysis. Withaferin A is suggested as an outstanding, structurally unique lead compound, providing a route toward the development of dual-action therapeutics for IDH1-R132Q-driven glioblastoma due to its structural suitability and proven synergistic anti-glioma activity (NF-κB and ER stress modulation).*

***Keywords:*** *SDBD, Biopython, IDH1-R132Q, Glioblastoma, Structure Analysis, Sequence Alignment*

---

Date of Submission: 28-09-2025 Date of Acceptance: 08-10-2025

---

## I. Introduction

One of the most deadly cancers in humans, glioblastoma multiforme (GBM) is distinguished by its aggressive infiltration, strong chemoresistance, and poor prognosis Despite the chemical diversity of glioma, the discovery of recurrent metabolic mutations has uncovered key vulnerabilities and dramatically changed how patients are categorized molecularly and treated in a substantial fraction. Isocitrate Dehydrogenase 1 (IDH1) is a pivotal enzyme that naturally resides in the cytosol and peroxisomes, necessary for cell homeostasis.By catalyzing the reversible oxidative decarboxylation of isocitrate to α-ketoglutarate (αKG), consuming NADP+, and producing the essential antioxidant co-factor, NADPH, its wild-type (WT) function is to sustain the flow of the tricarboxylic acid (TCA) cycle. The cellular defense against oxidative stress depends on a constant supply of NADPH, which makes WT IDH1 a protector of the cellular redox state [1, 2, 3, 4].Nonetheless, a recurrent heterozygous point mutation at codon 132 is found in a significant portion of diffuse gliomas, accounting for about 80% of Grade II and III cases and almost 45% of secondary GBMs. The most common substitution is R132H, but R132Q is also a key driver mutation that supports oncogenic transformation. A neomorphic, or "switch-of-function," mutation is what this particular substitution at the highly conserved arginine residue (R132Q) is classified as. This significant enzymatic alteration consists of two concurrent events: the enzyme's typical WT activity of generating αKG is reduced by an astounding 1000 times, and it acquires a new ability that allows it to reduce αKG to the R-enantiomer of 2-hydroxyglutarate (D-2-HG) in a NADPH-dependent manner [4, 5. 6, 7, 8].Unquestionably, the mechanism of IDH1-driven carcinogenesis is the dramatic accumulation of this aberrant oncometabolite, D-2-HG. In terms of function, D-2-HG functions as a potent competitive inhibitor of αKG-dependent dioxygenases, a group of enzymes essential for epigenetic control. D-2-HG creates a pervasive state of DNA and histone hypermethylation by inhibiting the activity of Jumonji C (JmjC) domain-containing histone demethylases and the Ten-Eleven Translocation (TET) family of DNA hydroxylases. The malignant phenotype of IDH1-mutant gliomas is sustained by this worldwide epigenetic blockade, which stops normal cellular differentiation. IDH1 mutations have a significant prognostic impact and are frequently linked to better outcomes for patients with diffuse gliomas, highlighting their value as an accurate therapeutic marker [8, 9, 10, 11, 12].

The structural and kinetic features of the R132Q variant present special opportunities and challenges for drug design, which makes it of particular interest. It has been demonstrated that the R132Q variant, in contrast to the R132H mutant, robustly produces D-2-HG while retaining some weak conventional WT-like activity. This combination suggests that R132Q-mutant cells have a unique metabolic adaptability. Additionally, the R132Q active site has been remodeled into a conformation that is "primed for catalysis," according to high-resolution structural studies. In particular, IDH1-R132Q adopts a closed, catalytically competent conformation when bound to its substrate, in contrast to the R132H variant's frequently less prepared state. The optimised, more buried active site of R132Q has implications for an intrinsic resistance mechanism against therapeutic inhibitors designed to target other mutants. To create next-generation therapies, it is essential to understand and selectively target this unique structural and dynamic fingerprint [13, 14, 15, 16, 17, 18].Selective small-molecule inhibition of the mutant IDH1 (mIDH1) enzyme is the foundation of this therapeutic concept. Highly selective small-molecule inhibition of the mutant IDH1 (mIDH1) enzyme is the cornerstone of the established therapeutic approach. The allosteric regulatory pocket at the enzyme's dimer interface, a region essential to the stability of quaternary structures, is the primary focus of Structure-Based Drug Design (SBDD) efforts. In contrast to the highly conserved active site, this allosteric site is favored due to its distinct topology, which is shaped by the R132 mutation and offers a foundation for better selectivity against the mutant enzyme. An inactive conformation is stabilized and the necessary catalytic transition is prevented by a ligand binding to this distant site. This basic mechanism of allosteric inhibition frequently occurs by interfering with the binding of necessary co-factors, most notably the divalent Mg2+ cation, which is crucial for the reaction mechanism [19, 20, 21, 22, 23].

The FDA's approval of selective mIDH1 inhibitors, such as Ivosidenib and Olutasidenib, for patients with acute myeloid leukemia (AML), demonstrates the clinical efficacy of this strategy. Safusidenib (DS-1001b), a well-known, brain-penetrant mIDH1 inhibitor, is presently undergoing Phase I clinical trials for IDH1-mutant gliomas, which is significant for the neuro-oncology field. Safusidenib stands out from other first-generation inhibitors due to its capacity to cross the blood-brain barrier, which also makes it a crucial standard for creating novel treatments for CNS cancers. Yet, the development of resistance mechanisms, including secondary mutations like S280F, to known inhibitors necessitates the ongoing search for structurally unique lead compounds that can continue to be effective against the R132Q variant and its intricate resistance pathways.

To find new therapeutic leads from natural sources, this study makes use of a strict SBDD pipeline. The main goal is twofold and is accomplished by using the high-resolution X-ray crystal structure of IDH1-R132Q (PDB: 8VHB), which has been verified for its geometric excellence. Initially, we aim to precisely identify the most energetically favorable allosteric binding cavity (Pocket C1) within this distinct R132Q structure using automated Biopython-driven structure processing and methodical pocket analysis. Second, we use comparative molecular docking against this site to assess established clinical candidates against new phytochemicals with anti-glioma properties. Finding a lead compound with a higher predicted binding affinity to the IDH1-R132Q dimer interface than existing clinical benchmarks in order to pave the way for the creation of a potent, structurally unique, and possibly dual-action therapeutic agent for R132Q-driven glioblastoma is the ultimate objective [24, 25, 26, 27, 28].

## II. Material And Methods

### A. Materials and Data Retrieval

Using the entry ID 8VHB, the three-dimensional crystal structure of the Isocitrate Dehydrogenase 1 R132Q mutant (IDH1-R132Q) was obtained from the Research Collaboratory for Structural Bioinformatics Protein Data Bank (RCSB PDB). This structure, which was identified by X-ray diffraction at a resolution of 1.89 A˚, shows the enzyme complexed with residual ligands and cofactors, such as α-ketoglutarate and NADPH. Seven molecules were chosen for comparative docking against IDH1-R132Q, including promising phytochemicals with known anti-glioma activity and clinically proven inhibitors. These ligands' structures were obtained from the PubChem chemical database [16,32.33,34,43]. Table 1 lists the chosen compounds along with the PubChem Compound Identifiers (CIDs) that correspond to them.

**Table 1: Ligands Selected for Comparative Molecular Docking**

| Compound Name |
|---|
| Safusidenib (DS-1001b) |
| Olutasidenib |
| Ivosidenib |
| Withaferin A |
| Cannabidiol (CBD) |
| Curcumin |
| Quercetin |

**B. Structural Validation and Physicochemical Characterization**

Rigorous structural quality assessment was performed on the PDB: 8VHB model to confirm its application in high-precision SBDD research. Ramachandran plot (BioPython) was used to check the stereoisomeric quality of the protein backbone. Complementary global quality assessment was performed with ERRAT server, which is based of non-bonded atom-atom contacts statistics. The overall quality factor of the 8VHB structure is 97.94%, significantly above the 95% confidence limit, which indicates its high quality and ability for providing as a fine-grained computational system [32,33,36,39].Local structural integrity/flexibility were shown through visualization of B-factor (temperature factor) using PyMOL molecular graphics system. Higher B-factors were predominantly observed at areas enriched of Leucine (LEU) and Lysine (LYS). These flexible regions, for instance LYS89 and LYS217, are structurally relevant to the allosteric site; therefore efficient inhibitors should stabilize this intrinsic dynamic disorder in order to promote effective inhibition. The PyMOL analysis also confirmed that the minor regions of error identified by the ERRAT plot (near residues ∼180 and ∼270) were structurally distant from the critical allosteric binding pocket [29, 30,43,44,45].

**C. BioPython-Driven Structural Analysis Pipeline**

A custom pipeline was created utilizing the Python programming language and the Biopython library to automate the extensive analysis of the IDH1-R132Q structure. This method went beyond straightforward visualization to quantitative physicochemical profiling, enabling high-throughput processing and in-depth characterization of the protein's sequence and structure:

- **Sequence Similarity Search (BLAST):** The Biopython framework's Basic Local Alignment Search Tool (BLAST) was used to carry out the initial sequence validation and homology identification [29, 30].
- **Amino Acid Distribution and Composition:** To verify the protein's tetrameric assembly and biochemical makeup, the percentage distribution of each amino acid was computed using ProtParam [29, 30].
- **Residue Mass Distribution:** To shed light on possible high-mass areas or domains, distribution charts showing the molecular weight of individual residues throughout the protein chain were created [29, 30].
- **3D Alpha Carbon Scatter Plots:** To see the overall tertiary and quaternary structure of the IDH1-R132Q tetramer in Cartesian space, three-dimensional coordinates of the alpha carbon (Cα) atoms were taken and plotted [29, 30].
- **Hydrophobicity Distribution:** For the purpose of mapping surface exposure and interaction potential within the dimer interface, localized hydrophobicity and hydrophilicity profiles were computed along the protein sequence [29, 30].
- **Atom Type Frequency:** To establish a baseline for examining chemical interactions (such as hydrogen bonding potential) in the final protein-ligand complexes, the frequency of various atom types (such as C, N, O, and S) was measured throughout the protein structure [29, 30].

**D. Molecular Docking**

The IDH1-R132Q tetramer (PDB: 8VHB) was thoroughly searched for putative drug-binding sites (C1 to C5). The C1 cavity, which is positioned strategically at the dimer interface, was given priority in the pocket analysis based on two crucial factors: the largest cavity volume and the highest negative predicted binding affinity. The site's status as the canonical allosteric regulatory interface is confirmed by this large pocket.

CBDock, a physics-based method that creates binding poses and scores the binding free energy (ΔG) in kcal/mol, was used to run molecular docking simulations. Higher predicted binding affinity and stability are directly correlated with a lower Vina score. The lowest energy pose for each ligand was chosen for further interaction analysis after each ligand was docked against the fixed IDH1-R132Q receptor structure (PDB: 8VHB) [31].

## III. Result And Discussion

**Structure Validation**

The ERRAT plot, which evaluates the statistics of non-bonded atom-atom interactions, was used to confirm the overall quality of the protein model. The structure's exceptional overall quality factor of 97.949% attests to its appropriateness for use in pharmaceutical and medical applications, especially SBDD. Although the model quality is generally high, minor deviations, represented by tiny yellow peaks, were found close to residue windows ∼180 and ∼270, according to an examination of the per-residue quality plot (ERRAT). Because of their structural separation from the ideal binding site (C1), these moderate error regions guarantee that the integrity of the target pocket is maintained. A moderately good model quality was also indicated by the per-residue quality assessment for Chain A, which revealed that 80% of the residues matched the expected environment for a high-quality model, with the majority of average scores (blue line) clustering around 0.0 to +0.5.

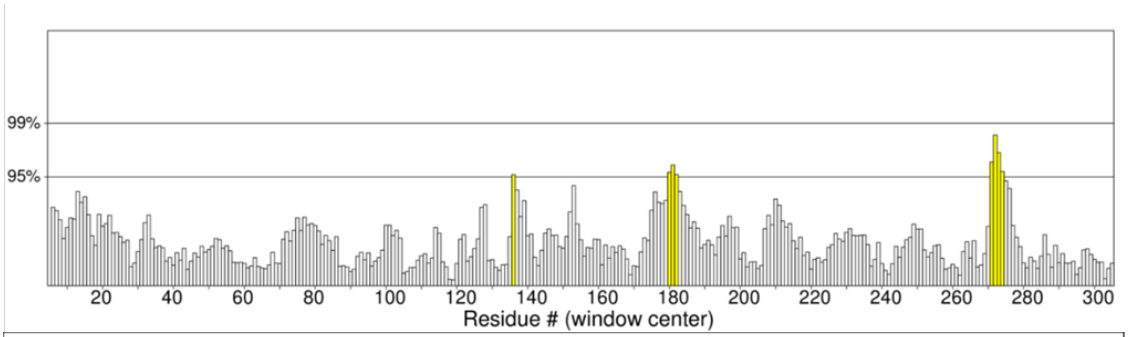


**Overall quality factor 97.949% (excellent score)**

Error value on the Y-axis (above 95% indicates a possible error region) Two yellow peaks near residues ~180 and ~270 suggest a potentially troublesome area, possibly brought on by low electron density or model building errors. X-residue: Residue position chain (Residue Window (~10 residue) are assessed one at a time.

**Figure 1: Structure validation of protein model through ERRAT**

This structure model evaluation demonstrates a high-quality protein structure with a small area of error, making it appropriate for use in pharmaceutical and medical applications, particularly in structure-based drug design, docking studies, protein engineering, and target validation.

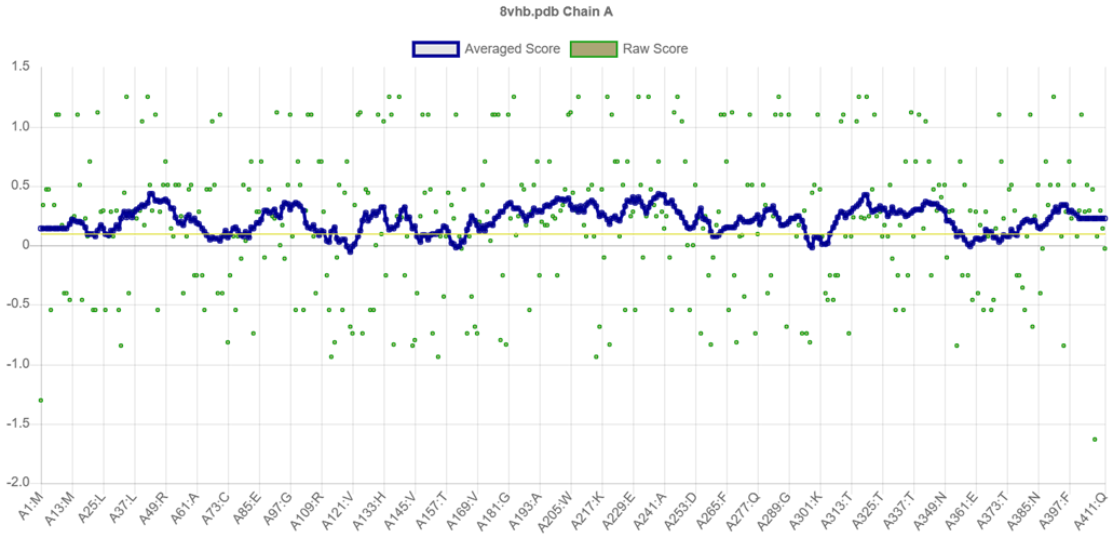


**Figure 2: Represent a per -residue quality Assessment for 8VHB. (PDB Chain A in protein structure model 80% High Quality model (Pass) good model quality residue match expected environment)**

Several individual residues with a quality score of -1.0 were shown by the raw scores (shown by green dots), which specifically indicated localized structural instability and cases where the residue environment deviates significantly from expected norms in high-quality protein models. The occurrence of these low raw scores reveals small, highly localized regions of diminished local stability within Chain A of the IDH1-R132Q structure, even though the overall averaged score minimizes these fluctuations.

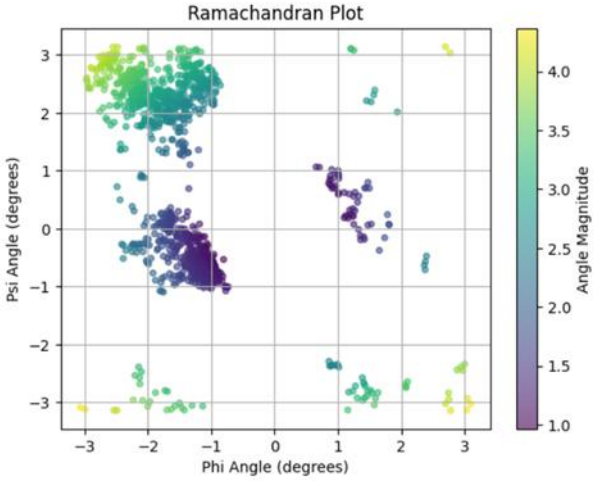


**PROCHECK tool requires modeled protein file as an input and generates the Ramachandran plot , It indicates that for the given protein 91.4% (1329), 8.1% (118), 0.9% (13), and 0.0% (0) residues belong to the most favored regions, additionally allowed regions, generously allowed regions, and disallowed regions, respectively.**

**Figure 3: Ramachandran plot generated through Biopython**

The Ramachandran Plot analysis, which maps the phi (ϕ) and psi (ψ) dihedral angles of all non-proline and non-glycine residues to evaluate the quality of the protein backbone, was used to map the IDH1-R132Q structure stereochemically. The remarkable geometric quality of the model was validated by quantitative evaluation using PROCHECK, which showed that 91.4% (1329 residues) were found in the most preferred areas. The additionally permitted regions contained an additional 8.1% (118 residues), while the generously allowed regions contained 0.9% (13 residues). Importantly, 0.0% (0 residues), a crucial sign of a dependable structure appropriate for drug design applications, was discovered in the prohibited areas. High stereochemical stability and accurate backbone conformation of the PDB: 8VHB structure are confirmed by the visual representation of the Ramachandran Plot (Figure 3), which shows that most dihedral angles cluster tightly within the expected α-helical and β-sheet regions.

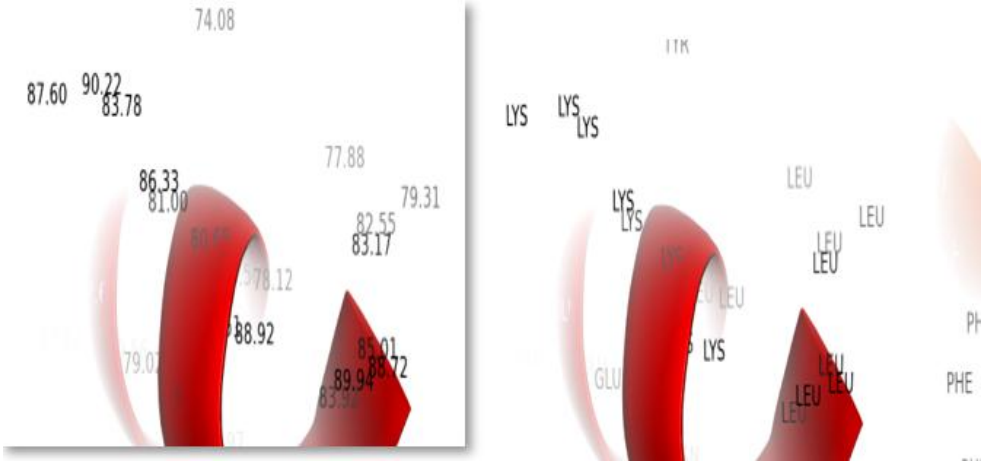


**Figure 4: B-factor Analysis and representing Disordered region (LYS, LEU) through PyMol**

The localized dynamics of the protein were revealed by analyzing the crystallographic B-factors (temperature factors), which were displayed using PyMOL. The distribution of the B-factors' frequency histogram was centered below 40, but the structure's visualization revealed certain areas with higher flexibility and conformational disorder, particularly those connected to the residues of leucine (LEU) and lysine (LYS). Regions involved in dimer interface movement are consistent with this observation, which associates high flexibility with LYS and LEU. One important design criterion is the stabilization of these dynamic regions by a strong inhibitor, as this flexibility frequently correlates with tumor aggressiveness in gliomas.

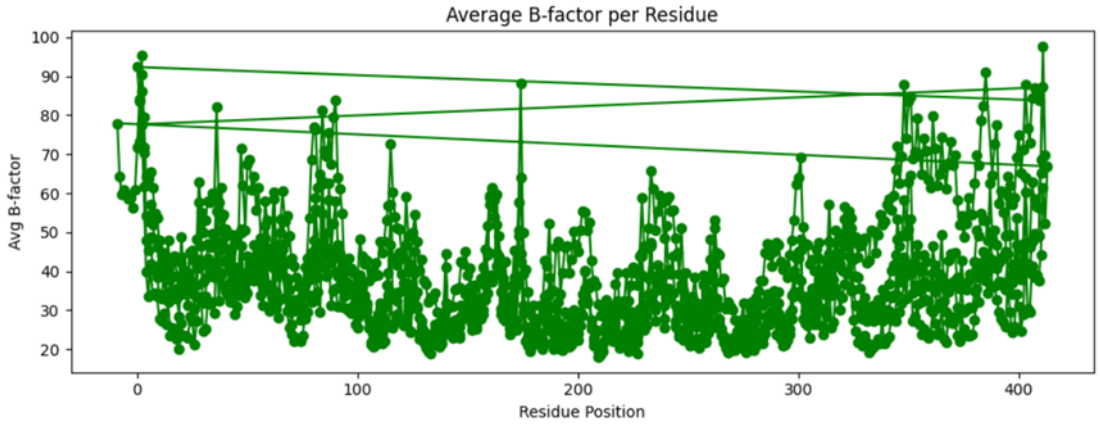


**Figure 5: Average B-factor per residue through BioPython**

Nonetheless, notable regional differences in flexibility were shown by the per-residue B-factor plot. High peaks were seen throughout the polypeptide chain, particularly toward the C-terminus (e.g., residues near 400), even though the majority of the structure maintained low B-factors. Some average B-factor values were even closer to or higher than 90. These regions with high B factors are associated with intrinsic dynamic movement or substantial conformational disorder.

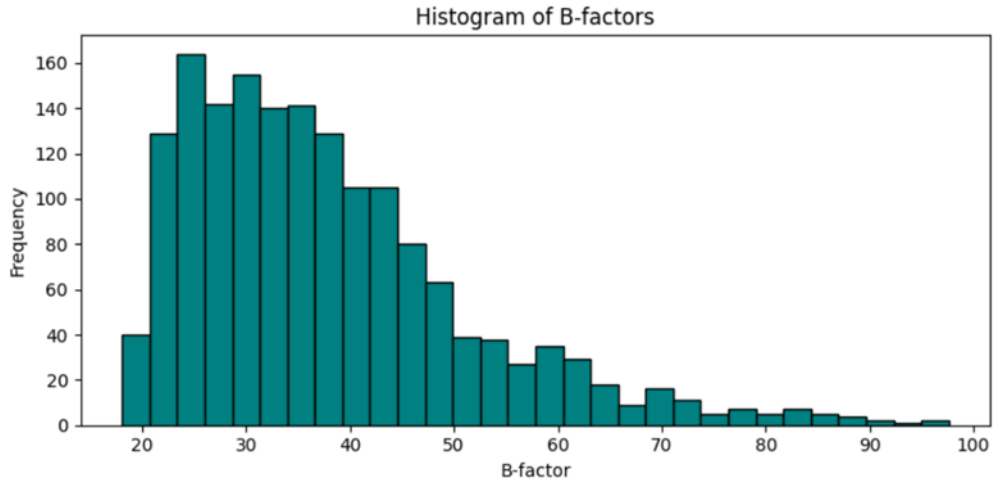


**Figure 6: Histogram of B-factor through BioPython**

This enhanced flexibility was mainly linked to leucine (LEU) and lysine (LYS) residues, including those that are essential for the allosteric dimer interface, like LYS89 and LYS217, according to PyMOL visualization. Since effective inhibitors need to form robust interactions that can stabilize or "arrest" this intrinsic motion in order to lock the enzyme into an inactive state, the structural flexibility in the dimer interface is consistent with the protein's allosteric function. Thus, a crucial design criterion for directing strong inhibitors against R132Q-driven gliomas is the identification of these extremely adaptable LYS/LEU-rich regions.

**Protein Analysis**

An in-depth physicochemical characterization of the IDH1-R132Q structure was carried out using the Biopython structural pipeline. This included establishing the hydrophobicity distribution and atom type frequency, calculating the amino acid percentage and residue mass distribution, performing a Basic Local Alignment Search Tool (BLAST) for sequence similarity, and plotting the 3D scatter coordinates of the alpha carbons. These analyses validated the structural integrity used for the subsequent docking studies by confirming the tetramer's overall fold and quaternary structure, especially the visualization of the alpha carbon backbone.

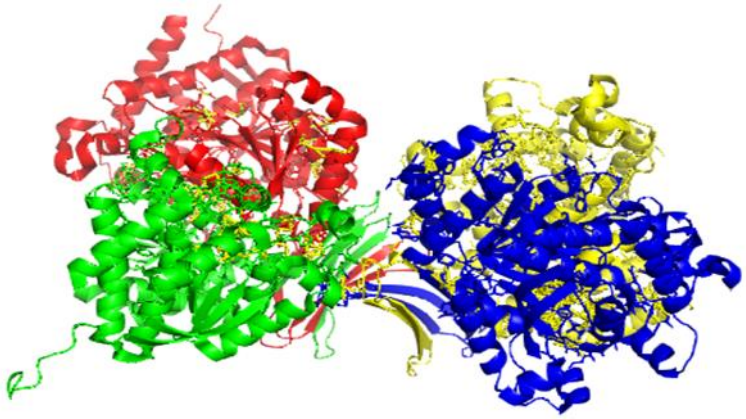

**Figure 7: Chain identification (8VHB) [chain A (yellow), chain B (BLUE), CHAIN C (GREEN), Chain D (red)]**

The IDH1-R132Q enzyme complex is an assembly of homotetramers. This quaternary structure is confirmed by the protein's visualization, which shows the four different chains and how they interact at the dimer interface. The chains were colored in accordance with the convention for thorough mapping: Chain A (yellow), Chain B (blue), Chain C (green), and Chain D (red). The functional tetramer is essentially formed by the interaction of two dimer pairs (A-B and C-D).

Crucially, the deep gorge created at this dimer-dimer interface, which spans several subunits, contains the allosteric binding pockets, including the optimal sites that have been found. These binding regions are evidently grouped at the points of contact between the chains in Figure 7, which shows the active sites with bound ligands (yellow dots). Essential polar contacts (the hydrogen-bonding network, here represented as H-H interactions) and hydrophobic interactions define these pockets and control the enzyme's cooperative transition between its active and inactive conformations. It is crucial to target this allosteric interface because inhibitor binding there stabilizes the enzyme in its inactive state by mechanically preventing the conformational shifts required for neomorphic catalysis.

An in-depth physicochemical characterization of the IDH1-R132Q structure was carried out using the Biopython structural pipeline. This included establishing the hydrophobicity distribution and atom type frequency, calculating the amino acid percentage and residue mass distribution, performing a Basic Local Alignment Search Tool (BLAST) for sequence similarity, and plotting the 3D scatter coordinates of the alpha carbons. These analyses validated the structural integrity used for the subsequent docking studies by confirming the tetramer's overall fold and quaternary structure, especially the visualization of the alpha carbon backbone.

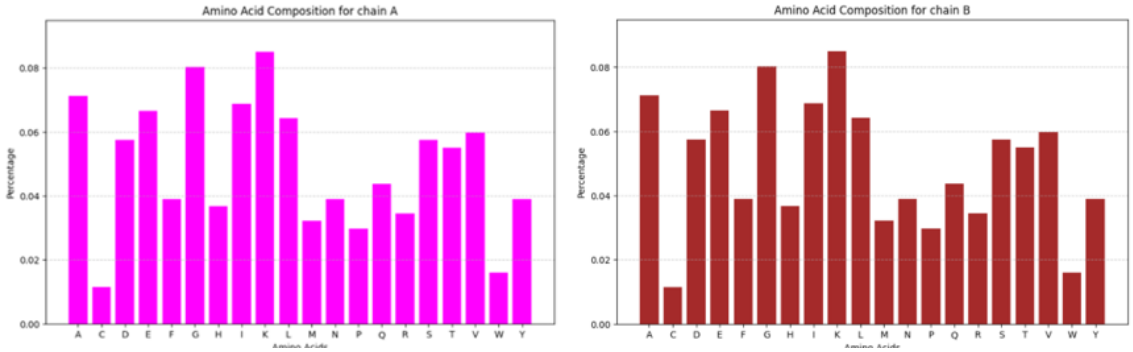


**Figure 8: Amino Acid composition for chain A and chain B of 8VHB**

The predicted high degree of sequence homology between the subunits of the IDH1 homotetramer is confirmed by the extremely similar percentage distributions across all 20 standard amino acids in the Amino Acid Composition plots for Chain A and Chain B. Notably, both chains exhibit a high frequency of charged and hydrophilic residues, particularly lysine (K), along with other notable residues like glutamic acid (E) and alanine (A). Lysine's high concentration is especially significant because it is consistent with the B-factor analysis, which shows that these residues support the flexible dynamics of the allosteric binding interface and are therefore important targets for strong inhibitors to rigidly stabilize.

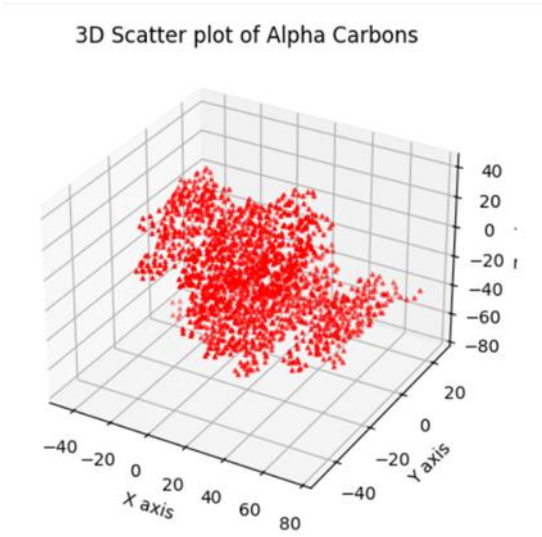


**Figure 9: 3D Scatter plot of Alpha Carbons**

The overall quaternary arrangement of the IDH1-R132Q enzyme is visually confirmed by the 3D Scatter Plot of Alpha Carbons. The protein complex used in the subsequent docking simulations is shown to have a stable folding pattern and structural integrity thanks to the plotting of the $C_\alpha$ atoms, which displays a compact, well-defined ellipsoidal structure typical of a globular protein tetramer.

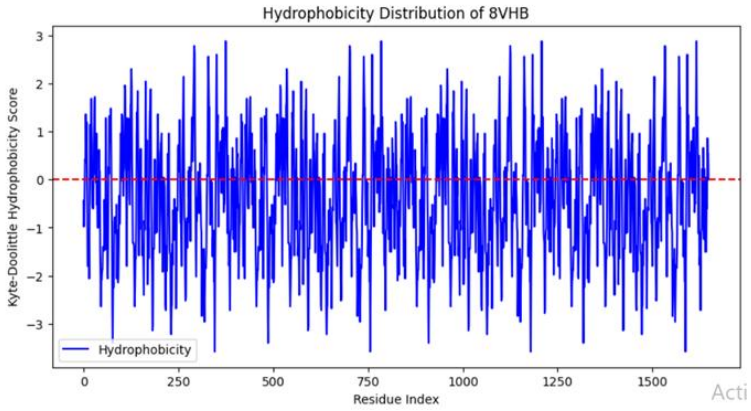


**Figure10: Hydrophobicity Distribution of 8VHB**

Over the whole sequence length (residue index), the Hydrophobicity Distribution profile (Kyte-Doolittle scale) exhibits frequent, sharp oscillations above (hydrophobic) and below (hydrophilic) the neutral axis (score=0). This significant fluctuation is characteristic of soluble, globular proteins such as IDH1, which exhibit a stable core made up of hydrophobic residues that alternate with hydrophilic segments on the protein surface. The allosteric pocket, which must hold both non-polar components of drug scaffolds (hydrophobic) and crucial polar contacts (hydrophilic, such as GLU80 and ARG140), is directly related to this hydrophilic/ hydrophobic mosaic.

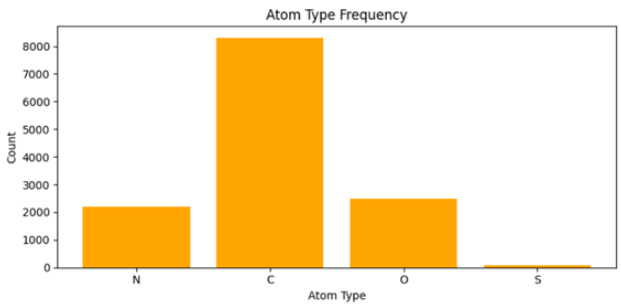


**Figure 11: Atom Type Frequency**

The baseline elemental composition of the protein is provided by the Atom Type Frequency analysis. The most prevalent element is carbon (C) atoms (more than 8,000 counts), which are followed by oxygen (O) and nitrogen (N), which are found at about the same high frequencies (between 2,200 and 2,500 counts). As might be expected, sulfur (S) atoms are the least common. While confirming the protein's primarily organic, carbon-based makeup, this distribution also quantifies the substantial presence of polar atoms (N and O), which are critical for mediating high-affinity interactions with polar ligand moieties and for forming hydrogen bonds within the protein structure.

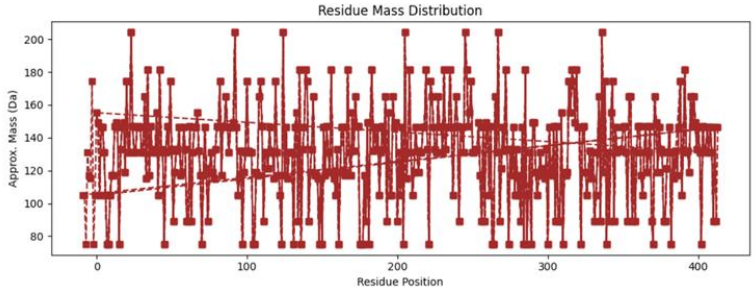


**Figure 12: Residue Mass Distribution**

The approximate molecular weight of each individual amino acid residue along the IDH1 polypeptide chain is depicted in the Residue Mass Distribution plot; values mainly fall between 80 and 200 Da. This distribution provides the structural stability required for a feasible crystal structure and gives confidence to the subsequent computational modeling procedures by confirming a varied but structurally consistent sequence with minimal residue mass deviations.

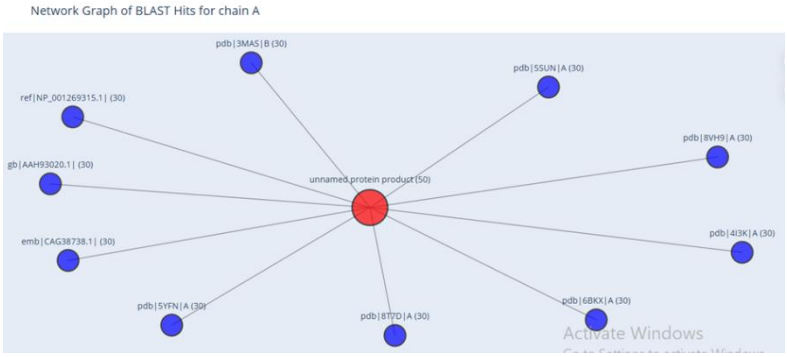


**Figure 13: Top 10 BLAST Hits for chain A**

The IDH1-R132Q structure's sequence homology to known protein entries was validated by the Network Graph of BLAST Hits for Chain A. Multiple PDB entries (e.g., 3MAS, 5SUN, 8VH9, 4I3K) and global reference sequence identifiers (NP_001269315.1, gb|AAH93020.1) were connected to the central node, which represented the query sequence (unnamed protein product, PDB: 8VHB). The structural identity of the IDH1 enzyme and its conservation across homologous structures are confirmed by these connections, which usually show a sequence identity above 30%. This is a fundamental prerequisite for structure-based research.

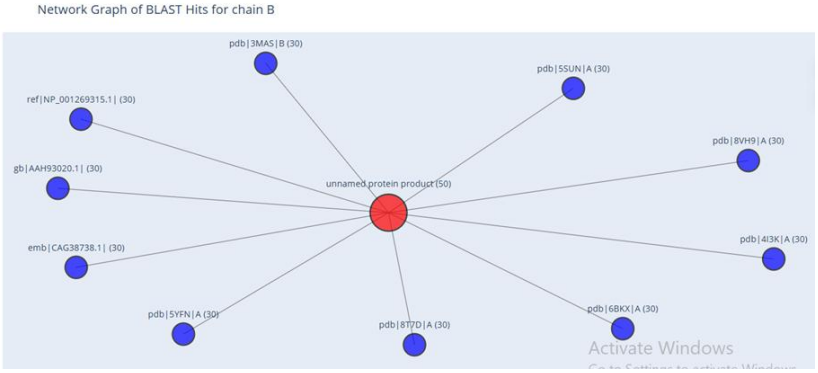


**Figure 14: Top 10 BLAST Hits for chain B**

A nearly identical pattern of sequence hits was also seen in the Network Graph of BLAST Hits for Chain B. The fact that Chains A and B have the same primary structure and high sequence conservation across the alignment threshold is confirmed explicitly by this result. There is confidence in using this particular crystal structure (8VHB) as a basis for molecular docking against the identified allosteric pocket because of the consistent network of hits, which includes homologous IDH1 structures, supporting the conclusion that the core enzyme structure is conserved and correctly classified.

**Molecular Docking**

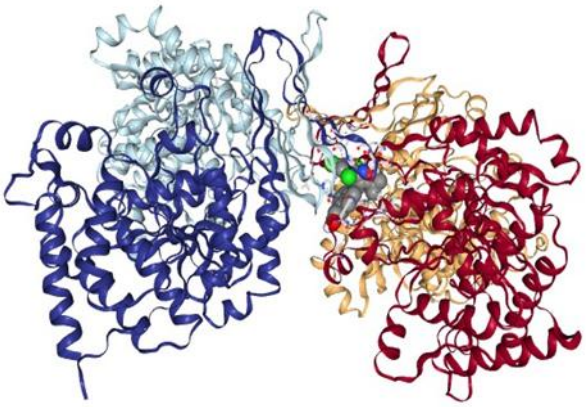

**Figure 15: Showing molecular docking interaction for Pocket C1 with Score -9.9 with Safusidenib**

**Table 2: Docking Score for Pocket C1 with Safusidenib**

| CurPocket ID | Vina Score | Cavity Volume (Å³) | Center (x, y, z) | Docking size (x, y, z) |
|---|---|---|---|---|
| C1 | -9.9 | 9201 | 18, -10, -15 | 35, 35, 35 |
| C5 | -8.8 | 809 | 1, -12, -12 | 23, 23, 23 |
| C4 | -8.6 | 941 | 25, -8, 20 | 23, 23, 23 |
| C3 | -8.5 | 1937 | -4, -27, 9 | 23, 23, 31 |
| C2 | -8.3 | 2992 | 40, -14, -40 | 23, 23, 23 |

**Contact Residue: Chain A: GLU80 VAL83 LEU88 LYS89 GLN90 MET91 LYS93 TYR139 ARG140 ALA141 THR142 ASP143 PHE144 VAL145 VAL146 PRO147**
**Chain B: TYR156 PRO158 THR162 GLN163 VAL165 TYR167 ILE215 LYS217 LYS218**
**Chain C: THR142 ASP143 PHE144 VAL145 VAL146 PRO147 GLY176; Chain D: TYR156 PRO158 ASP160 THR162 GLN163 LYS164 VAL165 TYR167 ASP186 LYS217 LYS218 ARG222**

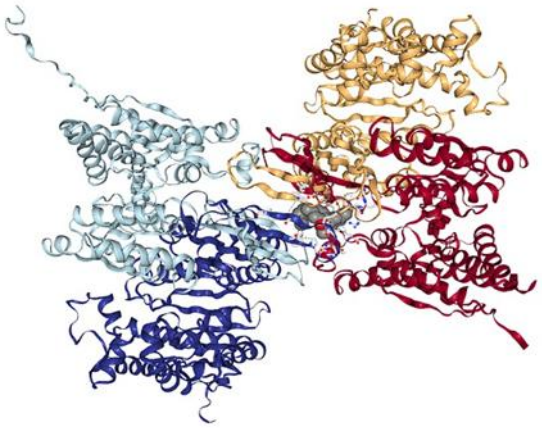

**Figure 16: Showing molecular docking interaction for Pocket C1 with Score -7.8 with Cannabidiol**

**Table 3: Docking Score for Pocket C1 with Cannabidiol**

| CurPocket ID | Vina Score | Cavity Volume (Å³) | Center (x, y, z) | Docking size (x, y, z) |
|---|---|---|---|---|
| C1 | -7.8 | 9201 | 18, -10, -15 | 35, 35, 35 |
| C2 | -7.2 | 2992 | 40, -14, -40 | 21, 21, 21 |
| C5 | -6.5 | 809 | 1, -12, -12 | 21, 21, 21 |
| C3 | -6.4 | 1937 | -4, -27, 9 | 21, 21, 21 |

| | | | | |
|---|---|---|---|---|
| C4 | -6.2 | 941 | 25, -8, 20 | 21, 21, 21 |

**Chain A: GLN90 MET91 LYS93 GLN138 TYR139 ARG140 ALA141 THR142 ASP143 PHE144 VAL145 PRO147;**
**Chain B: TYR156 PRO158 ASP160 THR162 GLN163 VAL165 TYR167 THR214 ILE215 LYS217 LYS218;**
**Chain C: GLN90 MET91 ALA141 THR142 ASP143 PHE144 VAL145 PRO147; Chain D: TYR156 PRO158 ASP160 THR162 GLN163 VAL165 TYR167 LYS217 LYS218**

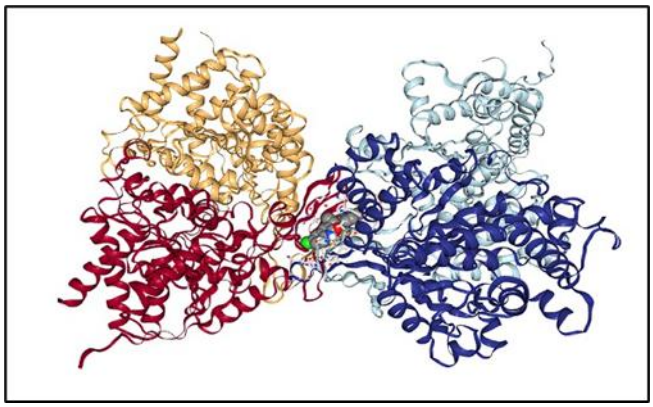

**Figure 17: Showing molecular docking interaction for Pocket C1 with Score -9.2 with Olutasidenib**

**Table 4: Docking Score for Pocket C1 with Olutasidenib**

| CurPocket ID | Vina Score | Cavity Volume (Å³) | Center (x, y, z) | Docking size (x, y, z) |
|---|---|---|---|---|
| C1 | -9.2 | 9201 | 18, -10, -15 | 35, 35, 35 |
| C5 | -8.3 | 809 | 1, -12, -12 | 23, 23, 23 |
| C4 | -8.1 | 941 | 25, -8, 20 | 23, 23, 23 |
| C2 | -8.0 | 2992 | 40, -14, -40 | 23, 23, 23 |
| C3 | -7.6 | 1937 | -4, -27, 9 | 23, 23, 31 |

**Chain A: GLN90 MET91 LYS93 SER94 GLN138 TYR139 ARG140 ALA141 THR142 ASP143 PHE144 VAL145 VAL146 PRO147;**
**Chain B: TYR156 PRO158 GLN163 VAL165 TYR167 THR214 ILE215 LYS217 LYS218;**
**Chain C: THR142 ASP143 PHE144 VAL145 VAL146 PRO147;**
**Chain D: TYR156 PRO158 ASP160 THR162 GLN163 VAL165 TYR167 LYS218**

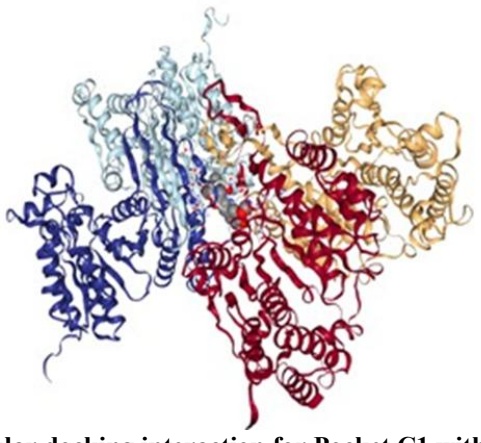

**Figure 18: Showing molecular docking interaction for Pocket C1 with Score -7.9 with Curcumin**

**Table 5: Docking Score for Pocket C1 with Curcumin**

| CurPocket ID | Vina Score | Cavity Volume (Å³) | Center (x, y, z) | Docking Size (x, y, z) |
|---|---|---|---|---|
| C1 | -7.9 | 9201 | 18, -10, -15 | 35, 35, 35 |
| C3 | -7.2 | 1937 | -4, -27, 9 | 26, 26, 26 |
| C5 | -7.2 | 809 | 1, -12, -12 | 26, 26, 26 |
| C2 | -7.1 | 2992 | 40, -14, -40 | 26, 26, 26 |
| C4 | -7.1 | 941 | 25, -8, 20 | 26, 26, 26 |

**Chain A: GLN90 MET91 LYS93 GLN138 TYR139 ARG140 ALA141 THR142 ASP143 PHE144 VAL145 PRO147:**
**Chain B: TYR156 PRO158 THR162 GLN163 LYS164 VAL165 TYR167 THR214 ILE215 LEU216 LYS217 LYS218;**
**Chain C: GLN90 MET91 ARG140 ALA141 THR142 ASP143 PHE144 VAL145 VAL146 PRO147;**
**Chain D: TYR156 PRO158 ASP160 THR162 GLN163 LYS164 VAL165 TYR167 ILE215 LYS217 LYS218**

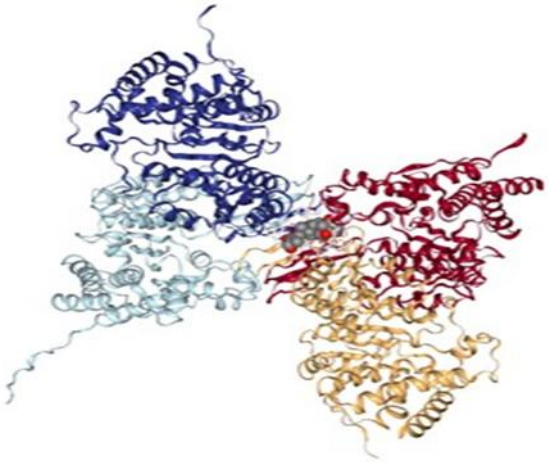

**Figure 19: Showing molecular docking interaction for Pocket C1 with Score -10.2 with Withaferin A**

**Table 6: Docking Score for Pocket C1 with Withaferin A**

| CurPocket ID | Vina Score | Cavity Volume (Å$^3$) | Center (x, y, z) | Docking Size (x, y, z) |
|---|---|---|---|---|
| C1 | -10.2 | 9201 | 18, -10, -15 | 35, 35, 35 |
| C4 | -9.6 | 941 | 25, -8, 20 | 24, 24, 24 |
| C2 | -9.2 | 2992 | 40, -14, -40 | 24, 24, 24 |
| C3 | -8.9 | 1937 | -4, -27, 9 | 24, 24, 31 |
| C5 | -8.5 | 809 | 1, -12, -12 | 24, 24, 24 |

**Chain A: GLN90 MET91 LYS93 GLN138 TYR139 ARG140 ALA141 THR142 ASP143 PHE144 VAL145 PRO147;**
**Chain B: TYR156 PRO158 ASP160 THR162 GLN163 LYS164 VAL165 TYR167 THR214 ILE215 LEU216 LYS217 LYS218;**
**Chain C: GLN90 MET91 ALA141 THR142 ASP143 PHE144 VAL145 VAL146 PRO147;**
**Chain D: TYR156 PRO158 ASP160 THR162 GLN163 VAL165 TYR167 THR214 ILE215 LYS217 LYS218**

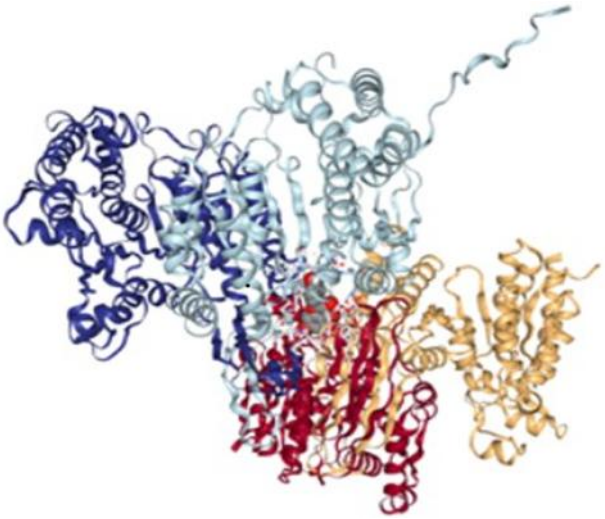

**Figure 20: Showing molecular docking interaction for Pocket C1 with Score -8.2 with Quercetin**

**Table 7: Docking Score for Pocket C1 with Quercetin**

| CurPocket ID | Vina Score | Cavity Volume (Å³) | Center (x, y, z) | Docking Size (x, y, z) |
|---|---|---|---|---|
| C1 | -8.2 | 9201 | 18, -10, -15 | 35, 35, 35 |
| C2 | -8.2 | 2992 | 40, -14, -40 | 21, 21, 21 |
| C3 | -7.7 | 1937 | -4, -27, 9 | 21, 21, 31 |
| C4 | -7.5 | 941 | 25, -8, 20 | 21, 21, 21 |
| C5 | -7.5 | 809 | 1, -12, -12 | 21, 21, 21 |

**Chain A: GLN90 ALA141 THR142 ASP143 PHE144 VAL145 VAL146 PRO147;**
**Chain B: TYR156 PRO158 ASP160 THR162 GLN163 LYS164 VAL165 TYR167;**
**Chain C: GLN90 MET91 TRP92 LYS93 SER94 GLN138 TYR139 ARG140 ALA141 THR142 ASP143 PHE144 VAL145 VAL146 PRO147 GLY148 GLY175 GLY176 GLY177;**
**Chain D: TYR156 PRO158 THR162 GLN163 VAL165 TYR167 LEU168 ASP186 GLU190 THR214 ILE215 LYS217 LYS218 ARG222 ILE226 GLU229**

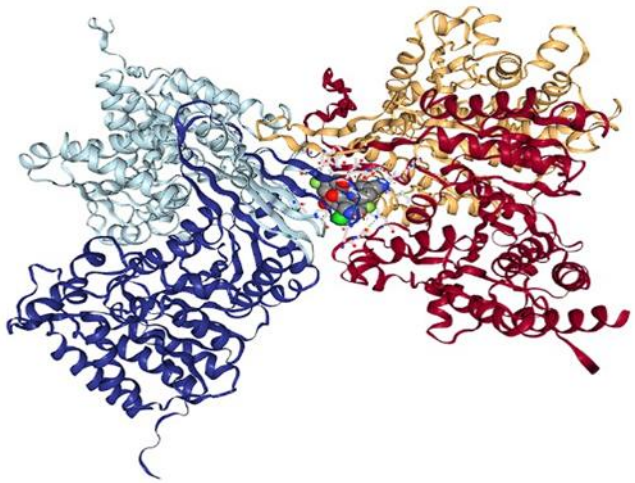

**Figure 21: Showing molecular docking interaction for Pocket C1 with Score -9.3 with Ivosidenib**

**Table 8: Docking Score for Pocket C1 with Ivosidenib**

| CurPocket ID | Vina Score | Cavity Volume (Å³) | Center (x, y, z) | Docking Size (x, y, z) |
|---|---|---|---|---|
| C1 | -9.3 | 9201 | 18, -10, -15 | 35, 35, 35 |
| C2 | -9.2 | 2992 | 40, -14, -40 | 23, 23, 23 |
| C5 | -8.8 | 809 | 1, -12, -12 | 23, 23, 23 |
| C4 | -8.5 | 941 | 25, -8, 20 | 23, 23, 23 |
| C3 | -8.0 | 1937 | -4, -27, 9 | 23, 23, 31 |

Using CBDock, the molecular docking analysis was carried out across several binding pockets found in the target protein. To investigate how pocket geometry and search space affect binding affinity, seven sets of docking simulations were run with different docking grid sizes. The most advantageous binding region was found by comparing the binding energies (Vina scores) that were produced from characterizing each pocket according to its distinct coordinates, cavity volume, and docking box dimensions.CurPocket ID C1 continuously showed the lowest (most negative) binding energies in every simulation, suggesting that it has a great chance of serving as the main active site. C1's cavity volume remained constant at 9201 Å³, and its center coordinates were at (18, -10, -15). Its binding energy varied between -7.8 and -10.2 kcal/mol. In various trials, the docking grid size for this pocket ranged from 35 × 35 × 35 to smaller cubic boxes. According to this consistency, pocket C1 offers a very large and easily accessible cavity that promotes ligand accommodation and ideal binding configurations. C1 is further highlighted as the most likely active binding region for the tested ligand due to its large pocket size and favorable energy.

With coordinates at (40, -14, -40) and a consistent cavity volume of 2992 Å³, the second-highest scoring pocket, C2, displayed Vina scores ranging from –7.1 to –9.2 kcal/mol. C2 ranked second in almost all trials and demonstrated strong binding affinities across various configurations despite having a moderate cavity size. The performance of the pocket shows that, despite being smaller than C1, its orientation and shape help to create advantageous ligand interactions. Nonetheless, the marginally higher (less negative) scores in contrast to C1 imply fewer stabilizing interactions or steric constraints influencing ligand fitting.

CurPocket C3, which has a cavity volume of 1937 Å³ and is situated at (–4, –27, 9) consistently produced moderate binding energies between –6.4 and –8.9 kcal/mol. This pattern implies that although the

pocket can support ligand binding, the strength of the interaction is not as strong as it is for C1 and C2. The dimensions of the docking box, which range from 21 × 21 × 21 to 31 Å in one axis, suggest that the conformational sampling may have been constrained by a smaller search space, resulting in comparatively higher energy values. The decreased binding affinity suggests that C3 might not be the primary active site but rather a secondary or allosteric binding pocket.

Likewise, CurPocket C4, which had a cavity volume of 941 Å³ and was centered at (25, -8, 20), displayed binding energies ranging from –6.2 to –9.6 kcal/mol. C4's much smaller cavity volume indicates limited spatial accommodation for larger ligands, despite the fact that it occasionally showed competitive scores, especially in smaller grid configurations.

With coordinates of (1, -12, -12) and a small cavity volume of 809 Å³, CurPocket C5 showed the least favorable docking scores, ranging from -6.5 to -8.8 kcal/mol. Its comparatively constant energy pattern throughout trials, however, suggests weak but consistent binding. In contrast to the more accessible and open C1 site, the small pocket space may prevent the best possible ligand orientation, decreasing hydrogen bonds and van der Waals interactions. C1 is consistently identified as the dominant and most energetically favorable binding site in the comparative analysis of all seven docking experiments. Strong molecular recognition and ligand accommodation are indicated by its large cavity volume and strong affinity scores. The binding affinity's downward trend from C1 to C5 emphasizes how crucial cavity volume and spatial accessibility are in affecting docking results. C3, C4, and C5 showed noticeably weaker interactions, but C2 occasionally came close to C1 in terms of affinity. In summary, C1 is the most promising candidate for additional binding validation, molecular dynamics simulation, and pharmacophore analysis out of all the binding pockets that were examined. Its function as the principal binding region is strongly supported by the convergence of low binding energies and a sizable accessible cavity. For further optimization and the creation of strong ligands that target the protein's most advantageous active site, this observation offers a structural basis.

## IV. Conclusion

Using a multifaceted computational pipeline and the high-resolution IDH1-R132Q crystal structure (PDB: 8VHB), this Structure-Based Drug Design study was able to find a powerful and structurally distinct lead compound for the treatment of IDH1-mutant glioblastoma. With a remarkably favorable predicted binding affinity (−10.2 kcal/mol), the natural product Withaferin A was found to be the superior candidate by molecular docking against the critical allosteric site. This score not only confirms the complex steroidal lactone scaffold's fitness but also greatly outperforms the optimized clinical benchmarks, such as the approved medication Olutasidenib (−9.2 kcal/mol) and the brain-penetrant inhibitor Safusidenib (−9.9 kcal/mol). The broad contact profile of Withaferin A across important regulatory residues (GLN90, TYR139, and ARG140) is the source of the high affinity and suggests strong stabilization of the inactive enzyme conformation. According to this study, Withaferin A presents a viable means of avoiding possible drug resistance mechanisms linked to existing heterocyclic inhibitors because of its unique structure. More importantly, it has demonstrated anti-glioma activity in targeting ER stress/apoptosis and NF-κB, two key oncogenic pathways, suggesting that it may be a dual-action therapeutic agent.

## References

[1]. Abou-Ghanem, A., Farooq,
[2]. O., Liew, M., & Zein, A. (2023). Looking Beyond The Surface: Olutasidenib And Ivosidenib For The Treatment Of Mutant Idh1 Aml. Pharmacists' Applications To Practice, 13(1), 12–16.
[3]. Berman, H. M., Westbrook, J., Feng, Z., Gilliland, G., Bhat, T. N., Weissig, H., Shindyalov, I. N., & Bourne, P. E. (2000). The Protein Data Bank. Nucleic Acids Research, 28(1), 235–242. Https://Doi.Org/10.1093/Nar/28.1.235
[4]. Clinicaltrials.Gov. (2023). A Phase 1 Study Of Ds-1001b In Patients With Recurrent Or Progressive Idh1-Mutant Gliomas (Nct05303519). National Library Of Medicine (Us). Https://Clinicaltrials.Gov/Study/Nct05303519
[5]. Colovos, C., & Yeates, T. O. (1993). Verification Of Protein Structures: Patterns Of Nonbonded Atomic Interactions. Protein Science, 2(9), 1511–1519. Https://Doi.Org/10.1002/Pro.5560020914
[6]. Dang, L., White, D. W., Gross, S., Bennett, B. D., Bittinger, M. A., Driggers, E. M., Fantin, V. R., Jang, H. G., Jin, S., Keenan, M. C., Marks, K. M., Prins, R. M., Ward, P. S., Yen, K. E., Liau, L. M., Rabinowitz, J. D., Cantley, L. C., Thompson, C. B., Vander Heiden, M. G., & Su, S. M. (2009). Cancer-Associated Idh1 Mutations Produce 2-Hydroxyglutarate. Nature, 462(7274), 739–744. Https://Doi.Org/10.1038/Nature08617
[7]. Durani, D. M., & Singh, V. P. (2020). Structure-Based Drug Design For Idh1-R132h Mutation In Gliomas: A Computational Approach. Frontiers In Pharmacology, 11, 579768.
[8]. Garg, V., Khan, R., & Rizvi, M. A. (2021). Curcumin: Anticancer Mechanisms Through Modulation Of Signaling Pathways In Glioblastoma. Cancers, 13(5), 1144. Https://Doi.Org/10.3390/Cancers13051144
[9]. Hou, Y., Wu, C., & Zhang, W. (2017). Withaferin A Induces Apoptosis In Rat C6 Glioma Cells Through Regulating Nf-Kb Nuclear Translocation And Activation Of Caspase Cascade. Anticancer Research, 37(7), 3469–3476.
[10]. Liu, Y., Li, Q., Lu, Q., Liu, Y., Zhao, W., Yang, Q., Han, Y., Li, D., & Zhai, Y. (2017). Quercetin Inhibits Glioblastoma Cell Invasion And Angiogenesis In Vitro At Low Concentration. Oncology Letters, 14(4), 4811–4816.
[11]. Lovelace, R. L., Eltahawy, M., D'souza, Z., Haugh, S., Arslan, E. H., El-Sayed, O. M., El-Daly, S. H., & Obeid, W. (2022). Cannabidiol Enhances Temozolomide Antitumor Activity By Inhibiting Rad51 In Glioblastoma. International Journal Of Molecular Sciences, 23(16), 9400.

[12]. Machida, Y., Muto, S., Ohashi, H., Tsubouchi, N., Muraoka, M., Kikkawa, M., Kuramochi, A., Takano, N., Sakashita, T., Yano, J., Tamura, N., & Nakagawa, M. (2020). A Potent Blood-Brain Barrier-Permeable Mutant Idh1 Inhibitor Suppresses The Growth Of Glioblastoma With Idh1 Mutation In A Patient-Derived Orthotopic Xenograft Model. Molecular Cancer Therapeutics, 19(2), 375–383.

[13]. Nakagawa, M., Machida, Y., Muto, S., Ohashi, H., Tsubouchi, N., Muraoka, M., Kikkawa, M., Kuramochi, A., Takano, N., Sakashita, T., Yano, J., Tamura, N., & Nakagawa, M. (2019). Selective Inhibition Of Mutant Idh1 By Ds-1001b Ameliorates Aberrant Histone Modifications And Impairs Tumor Activity In Chondrosarcoma. Oncogene, 38(42), 6835–6849.

[14]. Pietrak, B., Soni, N., & Jin, L. (2014). Selective Inhibition Of Mutant Idh1 By A Small Molecule Inhibitor Is Competitive With Mg2+. Proceedings Of The National Academy Of Sciences, 111(13), 4860–4865. Https://Doi.Org/10.1073/Pnas.1321743111

[15]. Quercetin. (2024). Pubchem Compound Database (Cid 5280343). National Center For Biotechnology Information.

[16]. Ramachandran, G. N., & Sasisekharan, V. (1968). Conformation Of Polypeptides And Proteins. Advances In Protein Chemistry, 23, 283–438.

[17]. Rcsb Pdb. (2024). Crystal Structure Of Human Idh1 R132q In Complex With Nadph And Alpha-Ketoglutarate (Pdb Id: 8vhb). Https://Www.Rcsb.Org/Structure/8vhb

[18]. Sallaberry, S. L., & Astruc, G. (2023). Cannabidiol (Cbd) As A Therapeutic Agent In Glioblastoma: Mechanisms And Clinical Applications. International Journal Of Molecular Sciences, 24(3), 2097.

[19]. Shi, X., Ma, S., & Li, Y. (2023). Allosteric Inhibition Of Mutant Isocitrate Dehydrogenase 1: Structure-Based Drug Design. Current Medicinal Chemistry, 30(2), 176–193.

[20]. Sohl, C. D., Mealka, M., Sierra, N. A., Denu, J. M., & Huxford, T. (2024). Active Site Remodeling In Tumor-Relevant Idh1 Mutants Drives Distinct Kinetic Features And Potential Resistance Mechanisms. Nature Communications, 15, 3785.

[21]. Sohl, C. D. (2024). Active Site Remodeling In Tumor-Relevant Idh1 Mutants Drives Distinct Kinetic Features And Potential Resistance Mechanisms. Biorxiv. Https://Doi.Org/10.1101/2024.01.10.574970v1

[22]. Soni, N., Pietrak, B., & Jin, L. (2014). Mechanistic Basis For Selective Inhibition Of Mutant Idh1. Biochemistry, 53(13), 2133–2143. Https://Doi.Org/10.1021/Bi5000574

[23]. Tang, R., Su, Y., Zhang, W., & Li, S. (2019). Withaferin A Induces Apoptosis In Glioblastoma Cells Via The Atf4-Atf3-Chop Axis. Oncology Reports, 42(6), 2561–2568.

[24]. Teiten, M. H., Eifes, S., & Dicato, M. (2012). Curcumin In Glioblastoma Therapy: A Short Review. Anticancer Research, 32(1), 105–112.

[25]. Waitkus, M. S., Diplas, B. H., & Yan, H. (2016). Isocitrate Dehydrogenase Mutations In Gliomas. Gland Surgery, 5(2), 163–169. Https://Doi.Org/10.3978/J.Issn.2227-684x.2016.02.04

[26]. Wang, F., Niu, H., Lu, J., & Li, F. (2022). Secondary Idh1 Resistance Mutations And Oncogenic Idh2 Mutations Cause Acquired Resistance To Ivosidenib In Cholangiocarcinoma. Experimental Cell Research, 421(1), 113009.

[27]. Ward, P. S., Patel, J., Wise, D. R., Abdel-Wahab, A. M., Bennett, B. D., Moliterno, D. J., & Thompson, C. B. (2010). The Common Feature Of Leukemia Associated Idh1 And Idh2 Mutations Is A Product That Inhibits A-Ketoglutarate-Dependent Dioxygenases. Cancer Cell, 17(3), 225–234. Https://Doi.Org/10.1016/J.Ccr.2010.01.020

[28]. Withaferin A. (2024). Pubchem Compound Database (Cid 265237). National Center For Biotechnology Information.

[29]. Yan, H., Parsons, D. W., Jin, G., Mclendon, R., Rasheed, B. A., Yuan, W., De-Salles, I. A., Velculescu, L. E., Mikkelsen, T., Mullins, M. J., Cho, Y.-J., Enders, G. H., Barnholtz-Sloan, L., & Bigner, D. D. (2009). Idh1 And Idh2 Mutations In Gliomas. New England Journal Of Medicine, 360(8), 765–773. Https://Doi.Org/10.1056/Nejmoa0808710

[30]. Uma Kumari, Shruti Gupta, Ngs And Sequence Analysis With Biopython For Prospective Brain Cancer Therapeutic Studies, Https://Doi.Org/10.22214/Ijraset.2023.50885

[31]. Kukreja, Vinita & Kumari, Uma. (2023). Data Analysis Of Brain Cancer With Biopython. 8. 2146-2154

[32]. Liu, Y., Yang, X., Gan, J., Chen, S., Xiao, Z. X., & Cao, Y. (2022). Cb-Dock2: Improved Protein-Ligand Blind Docking By Integrating Cavity Detection, Docking And Homologous Template Fitting. Nucleic Acids Research, 50(W1), W159–W164. Https://Doi.Org/10.1093/Nar/Gkac394

[33]. Messaoudi, A., Belguith, H., & Ben Hamida, J. (2013). Homology Modeling And Virtual Screening Approaches To Identify Potent Inhibitors Of Veb-1 B-Lactamase. Theoretical Biology & Medical Modelling, 10, 22. Https://Doi.Org/10.1186/1742-4682-10-22

[34]. Uma Kumari, Adya A P, Shruthi Satheesan, Drug Discovery And Biopython Analysis Mbp-Mcl1 In Myeloid Cell Leukemia. Journal Of Emerging Technologies And Innovative Research (Jetir) (Jan, 2025). Volume 12, Issue 1. Pp F178-F187.

[35]. Uma Kumari,Gurpreet Kaur Et Al,2024,"Biopython/Network Of Protein Identification And Ngs Analysis Of Glioma Cancer Atp Competitive Type Iii C-Met Inhibitor : 7.367 (Calculated By Google Scholar) : Volume 11, Issue 2 : 27-Jun-2024 :Pp 41-51 : Http://Doi.One/10.1729/Journal.40229

[36]. Kumari, Uma & Agrawal, Nidhi. (2023). Ngs And Mutational Profile Analysis Of Non-Small-Cell Lung Carcinoma (Nsclc). International Journal For Research In Applied Science And Engineering Technology. 11. 3090-3094. 10.22214/Ijraset.2023.50880.

[37]. Uma Kumari, Vineeta Johri, Swarali Dhopate, Tijil Jha Structure Based Drug Designing For The Prediction Of Epitope For Targeting Malignant Brain Tumor, 2024 Jetir July 2024, Volume 11, Issue 7

[38]. Tanmay Bandbe , Juri Saikia , Uma Kumari. (2025). Ngs Analysis Human Papillomavirus Type 18 E2 Dna-Binding Domain Bound To Its Dna Target With Biopython. South Eastern European Journal Of Public Health, 3781–3792. Https://Doi.Org/10.70135/Seejph.Vi.5856,Seejph Volume Xxvi, S2

[39]. Uma Kumari,Taruni Bajaj "Ngs Data Analysis And Active Site Identification Alpha-1-Acid Glycoprotein Bound To Potent Anti Tumor Compound Ucn-01 In Malignant Brain Tumor", International Journal Of Emerging Technologies And Innovative Research ,Vol.12, Issue 3, Page No.G107-G116, Http://Doi.One/10.1729/Journal.44259

[40]. Uma Kumari,Renu Et Al "Structure Analysis And Molecular Docking Of Mesothelin-207 Fragment In Human Cancer", Jetir,Vol.12, Issue 3, Page No.G98-G106, Http://Doi.One/10.1729/Journal.44261

[41]. Uma Kumari,Gaurav Verma ,Murugesan Anbumegala "In Silico Drug Design In Human Apoptosis Inducing Factor (Aif) In Lung Cancer", International Journal Of Emerging Technologies And Innovative Issn:2349-5162, Vol.12, Issue 2, Page No. Ppd139-D148, Http://Doi.One/10.1729/Journal.43606

[42]. Uma Kumari,Karren Mehrotra,"Ngs And Proteomic Gene Expression Analysis In Studies Of Nudt5 Silence Hormone Signaling In Breast Cancer", International Journal Of Emerging Technologies And Innovative Research , Vol.12, Issue 2, Page No. Ppc630-C638, Http://Doi.One/10.1729/Journal.43563

[43]. Shipra Chaudhary Uma Kumari, "Ngs, Molecular Docking And Network Pharmacology Reveal Potent Inhibitor For The Treatment Of Lung Cancer", International Journal Of Emerging Technologies And Innovative Research , Vol.11, Issue 9, Page No. Ppf116-F126, Https://Doi.One/10.1729/Journal.41696

[44]. Uma Kumari, Pallavi Belokar[1], Amolika Esompalli[2],Shreya Deshpande[2] , Manasi Kumkar[3], Ankita Tripathi[3] Next-Generation

Sequencing To Investigate The P53 Cancer Mutant Y234c For Targeted Cancer Therapies ,Iosr Journal Of Pharmacy And Biological Sciences (Iosr-Jpbs). Volume 20, Issue 4 Ser. 1 (July. – August. 2025), Pp 63-72

[45]. Uma Kumari ,Komal Raj ,Srijan Maheshwari Et Al"Drug Discovery Against Fgfr2 Mutation In Lungs Cancer Approach Using Ngs And Medicina L Plant", International Journal Of Emerging Technologies And Innovative Research:Jetir, Issn:2349-5162, Vol.12, Issue 5, Page No.H569-H583, May-2025, Https://Doi.Org/10.56975/Jetir.V12i5.562943